

## Publication I

Janne Halme, Minna Toivola, Antti Tolvanen, and Peter Lund. 2006. Charge transfer resistance of spray deposited and compressed counter electrodes for dye-sensitized nanoparticle solar cells on plastic substrates. *Solar Energy Materials & Solar Cells*, volume 90, numbers 7-8, pages 872-886.

© 2005 Elsevier Science

Reprinted with permission from Elsevier.



ELSEVIER

Available online at [www.sciencedirect.com](http://www.sciencedirect.com)

SCIENCE @ DIRECT®

Solar Energy Materials  
& Solar Cells

Solar Energy Materials & Solar Cells 90 (2006) 872–886

[www.elsevier.com/locate/solmat](http://www.elsevier.com/locate/solmat)

# Charge transfer resistance of spray deposited and compressed counter electrodes for dye-sensitized nanoparticle solar cells on plastic substrates

Janne Halme\*, Minna Toivola, Antti Tolvanen, Peter Lund

*Laboratory of Advanced Energy Systems, Department of Engineering Physics and Mathematics,  
Helsinki University of Technology, P. O. Box 2200, FIN-02015 TKK, Finland*

Received 2 February 2005; accepted 3 May 2005

Available online 13 June 2005

---

## Abstract

Electrochemical impedance spectroscopy was used to determine the effective charge transfer resistances of porous dye-sensitized solar cell counter electrodes prepared by low-temperature spray deposition and compression of conductive carbon and platinized Sb-doped SnO<sub>2</sub> powders on indium tin oxide-coated plastic substrates. The charge transfer resistances were 0.5–2 and 8–13 Ω cm<sup>2</sup>, respectively, when using 3-methoxypropionitrile as the electrolyte solvent. The manufacturing method used lends itself to produce mechanically stable and even-quality electrodes in an easy and fast manner.

© 2005 Elsevier B.V. All rights reserved.

*Keywords:* Dye-sensitized solar cell; Counter electrode; Plastic substrate; Impedance spectroscopy; Charge transfer resistance

---

## 1. Introduction

Over the past 10 years significant amount of research effort has been targeted worldwide to the development of dye-sensitized TiO<sub>2</sub> nanoparticle solar cells. Dye-sensitized solar cells (DSSCs) have certain advantages over conventional silicon and

---

\*Corresponding author. Tel.: +358 9 4513213; fax: +358 9 4513195.

E-mail address: [janne.halme@tkk.fi](mailto:janne.halme@tkk.fi) (J. Halme).

thin film photovoltaic devices. The possibility to low-cost PV production due to the simplicity of the manufacturing process and cost-effectiveness of most of the cell materials makes this type of solar cells interesting for mass production. The dye solar cell technology could be used on a short-term perspective for low-current electronic consumer applications, such as wearable electronics, electronic paper, smart labels, etc.

While the basic dye solar cell is often built on a glass substrate, technological and practical advantage could be gained if the dye solar cell concept could be successfully utilized with light and flexible substrates such as plastics and metal foils. This is also the general trend in the development of other thin film solar cells such as a-Si and CIGS. Plastic substrates are also well suited for continuous and high throughput manufacturing process, for example the so-called roll-to-roll manufacturing, used in the paper and coating industry.

This study concentrates on the preparation methods of counter electrodes (CEs) of dye solar cells made on plastic substrates and on their characterization by electrochemical impedance spectroscopy (EIS). The task of a CE in the DSSC is to return the charge from the external load to the electrolyte reducing the oxidized form of the iodide/triiodide redox couple in it and thus keeping the operating cycle of the cell running. The charge transfer resistance between the electrode and the electrolyte appears as a voltage loss at the CE and it contributes directly to the series resistance of the whole cell. This means that a good CE material must possess low charge transfer resistance (i.e. good electrocatalytic activity), but also good mechanical and chemical stability.

The most commonly used CE in DSSCs is a fluorine-doped tin oxide (FTO)-coated glass, deposited with a small amount of platinum, for example, by sputtering [1]. Papageorgiou et al. [2] developed a catalyst based on thermal decomposition of a platinum chloride precursor at about 400 °C. Because of its high electrocatalytic activity towards iodine/triiodide reduction at low Pt loading, chemical and mechanical stability, and easiness of preparation, it is widely used in dye solar cells based on glass substrates, but the high temperatures involved makes it incompatible with plastic substrates.

Carbon has been used as an alternative CE catalyst material to platinum [3–8]. The lower catalytic activity of carbon compared to platinum can be compensated by increasing the active surface area of the electrode by using porous electrode structure. Kay and Grätzel [3] achieved good solar cell performance in a monolithic cell construction on FTO glass with 60 µm thick porous electrodes made by depositing a powder mixture of graphite, carbon black and nanocrystalline TiO<sub>2</sub> and sintering at 450 °C. Burnside et al. [4] prepared similar electrodes by screen printing and Papageorgiou et al. [5] studied mass transport in the electrolyte in these porous electrodes. Imoto et al. [6] showed that with CEs based on high specific surface area-activated carbon materials and heat treated at 180 °C, solar cell performance comparable to platinum catalyst CEs could be reached. Carbon nanotubes have also been successfully used [7], and carbon black has been used to improve electrical contact between the CE and a polypyrrole hole transport layer in a solid-state DSSC [8].

Recently, conducting polymer poly(3,4-ethylenedioxythiophene) (PEDOT) doped with either *p*-toluenesulfonate (PEDOT-TsO) [9,10] or polystyrenesulfonate (PEDOT-PSS) [11] has been identified as an efficient CE catalyst material for DSSCs. These polymer electrodes are prepared at low temperature (110 °C or below) which is compatible with plastic substrates.

CEs on plastic substrates have usually been prepared by sputtering a small amount of platinum, e.g. [12–16]. Lindström et al. [17] developed an alternative method where the CE is prepared by compressing powder materials onto indium-doped tin oxide (ITO) coated polyethyleneterephthalate (PET) substrate at room temperature. Two types of materials were used in their study: either a graphite–carbon black–nanocrystalline TiO<sub>2</sub> mixture similar to that used for monolithic cells on FTO glass [3,4], but without heat treatment, or thermally platinized Sb-doped SnO<sub>2</sub> particles. Compared to vacuum sputtering of Pt, these compressed CEs offer an interesting alternative where the manufacturing of the CE sheets could be made in a high throughput continuous process at room temperature. These compressible CE materials were selected as the materials for the present study.

The goal of this work was to study how well the compressed powder CEs meet the demands for electrocatalytic activity and durability, and what are their prospects from the point of view of reliable and fast manufacturing process, the underlying motive being to eventually upscale DSSC production, including CE, from laboratory into industrial scale.

The powder materials were spray deposited onto flexible ITO–PET substrates and compacted at room temperature to yield porous CE films. The electrodes were employed in a thin layer cell configuration, and their overall charge transfer resistances were determined with EIS. Thermal platinum electrodes on FTO-coated glass were prepared and characterized for comparison.

The results show that the charge transfer resistances obtained with these materials are well competitive to those obtained with platinum on glass. The manufacturing process is easy and fast, yielding electrodes with even quality. The adherence to the substrates is adequate and tolerance to mechanical stress good during the cell manufacturing.

## 2. Experimental

### 2.1. Substrates

FTO glass (TEC 15 from Pilkington) with sheet resistance of about 15 Ω/sq. supplied by Hartford Glass Co. was used as the conductive substrate for thermal platinum CEs. ITO–PET (NV-CT-CHO1S-M-7) with sheet resistance of about 60 Ω/sq. and total film thickness of 190 μm supplied by Bekaert Specialty Films was used as the plastic substrate. The size of all substrates was 20 × 20 mm.

Before use, the substrates were washed first with warm water and mild detergent, then rinsed with distilled water, and finally dried in air. The cleaning was completed by placing the substrates in an ultrasonic bath at room temperature

first in ethanol and then in acetone for 3 min. Finally the substrates were dried with pressurized air.

## 2.2. Counter electrode materials

Two powder materials were tested and compared to thermal Pt. The preparation of the materials was done as follows:

- Carbon powder suspension: 0.8 g of graphite powder (synthetic, conducting grade, –325 mesh, supplied by Alfa Aesar) and 0.2 g of extra-conductive carbon black (Printex XE2, Degussa) were ground together in a mortar with 1 g of ethanol. 0.36 g of TiO<sub>2</sub> (P25, Degussa) was added after this, followed by 5 g of ethanol after which the mixture was stirred vigorously with a magnetic stirrer for minimum 12 h before use.
- Sb:SnO<sub>2</sub> + Pt powder suspension: 2 g of Sb-doped SnO<sub>2</sub> (Zelec ECP 3010-XC, Milliken Chemicals) was mixed with 2 ml of the platinum solution described below. The mixture was fired in an oven at 385 °C for 10–15 min. The resulting powder was crushed, mixed with 6 g of ethanol, and stirred with a magnetic stirrer for minimum 12 h before use. For comparison, a Sb:SnO<sub>2</sub> powder suspension was also prepared without the platinization.
- Pt solution: 16.7 mg of PtCl<sub>4</sub> (Aldrich) was dissolved into 10 ml of isopropanol (pro analysi, Merck), resulting in a platinum concentration of 5 mM.

## 2.3. Deposition

A mask made of transparency foil with a circular hole of 5 mm diameter resulting in an electrode area of 0.2 cm<sup>2</sup> was used to define the area of deposition. The spraying of both the powder suspensions and the platinum solution was done with an Aztec A320 airbrush placing the mask-covered substrate on a hot plate perpendicularly under the spray, at a distance of ca. 10 cm from the spray nozzle. The hot plate temperature was kept at about 100 °C which sped up the manufacturing process by vaporizing the solvent from the mixture right after deposition. It was noticed that the TiO<sub>2</sub> used as the binder in the carbon powder mixture tended to separate from the suspension, so the suspension had to be used when fresh, preferably in a couple of days from the preparation.

## 2.4. Compressing/firing

Compressing of the powder materials at room temperature was done between two stainless-steel plates with MTS 810 Material Test System hydraulic press. Kapton<sup>®</sup> polyimide foil (DuPont) for Sb:SnO<sub>2</sub> + Pt, and regular household aluminum foil for the carbon powder mixture were used to prevent the materials from sticking onto the press plates. Compressing force was either 40 or 60 kN, equaling 1000 or 1500 kg/cm<sup>2</sup> in pressure, respectively. No difference in the electrode quality or performance was noticed between these two pressures so 60 kN was used in the most cases.

Platinum electrodes were fired at 385 °C for 10–15 min to ensure proper adherence and activation of the catalyst. Firing was also tried at 150 °C for ITO–PET substrates but gave only poor results, even with firing times up to 24 h.

## 2.5. Measurement cells

The CE films were employed for impedance measurements in a symmetrical thin layer cell configuration used previously for this purpose also by others [2,10,18,19]. Fig. 1 depicts the geometry of the measurement cell, denoted hereafter as the CE–CE cell.

Impedance spectroscopy using the CE–CE cell configuration has several benefits for characterization of dye solar cell CEs. First of all, the CE–CE cell configuration is practical and relevant to the structure and preparation of the actual solar cell. The thinness of the electrolyte layer also eliminates contributions from convection to the ion transport. Compared to measurements with complete solar cells it allows characterization of the CEs independently from effects of the photoelectrode. This facilitates comparison between different studies where the properties of the photoelectrodes would likely to be different. Exclusion of the photoelectrode response also makes the interpretation of the impedance spectra more accurate and straightforward. A drawback of the CE–CE measurement configuration is the absence of a reference electrode that would make it possible to measure the current–potential characteristics of a single electrode. For the same reason EIS measurements are best done at zero polarization. When DC current flows the CE–CE cell is electrochemically asymmetric, the other electrode being polarized anodically and the other cathodically [18], which complicates the analysis of the measurement results in terms of overpotentials of a single electrode.

The CE–CE measurement cells were prepared in the following way. Two electrodes with film thickness and surface density of the electrode material close to each other were selected for each CE–CE cell. 60 μm thick Surlyn<sup>®</sup> 1702 ionomer

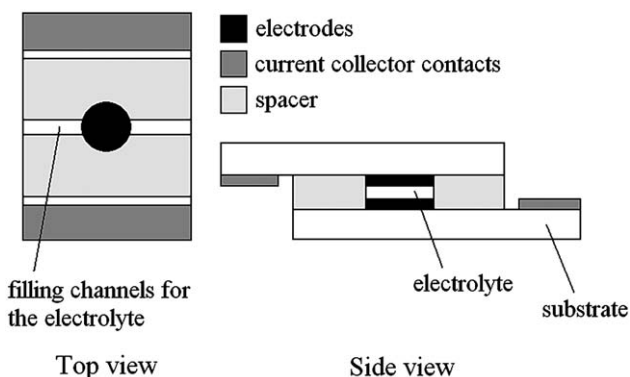


Fig. 1. Geometry of the CE–CE cells used for impedance measurement. The top view is approximately to scale, whereas the side view is schematic for clarity.

resin film (DuPont) was used as the spacer and sealing the substrates together. Cells were assembled on a hot plate heated to 100 °C with a constant pressure applied to melt the Surlyn film. After this the current collector contacts made of copper tape were placed on the both sides of the cell. Electrolube<sup>®</sup> conductive silver paint was used to further reduce the resistance between the conductive coating of the substrate and the copper tape.

Electrolyte was added via filling channels left in the spacer film after which the channel openings were sealed with TorrSeal<sup>®</sup> high vacuum sealant (Varian Vacuum Technologies). The cell was left for minimum 12 h at room temperature before further measurements. The electrolyte consisted of 0.5 M LiI, 0.05 M I<sub>2</sub> and 0.5 M (7.4 vol. %) *tert*-butyl-pyridine (TBP) in methoxypropionitrile, a composition widely used in DSSCs.

## 2.6. Measurements

Impedance spectra and current–voltage curves were recorded with Zahner Elektrik's IM6 Impedance Measurement Unit controlled with Thales software. Measurements were done at room temperature in the frequency range 100 mHz–100 kHz with 10 mV voltage amplitude at zero DC cell polarization. The cells were measured after preparation as soon as possible, usually the same or next day.

The thicknesses of the electrode films were measured after compressing with a Heidenhein Digitaler Messtaster MT12 thickness meter coupled to a Heidenhein ND 221 B display unit, and masses with a Mettler M3 scales, both before and after compressing.

## 3. Results and discussion

### 3.1. Interpretation of the measured electrochemical impedance spectra

Figs. 2 and 3 show typical impedance spectra of compressed carbon powder and Sb:SnO<sub>2</sub> + Pt electrodes measured using the cell configuration depicted in Fig. 1. The measured impedance spectra were dominated by two characteristic frequencies resulting in two impedance arcs in the Nyquist plot (Fig. 2) and correspondingly two peaks in the imaginary part of the impedance ( $-Z_{\text{Im}}$ ) vs. frequency plot (Fig. 3).

As justified by theoretical reasoning and experimental evidence discussed in detail in the subsequent Sections 3.2–3.4, the impedance spectra of the compressed CEs can be interpreted and modeled using the equivalent circuits shown in Fig. 4. Two different types of measurement cells are considered: Firstly, CE–CE –cells in which the substrate's ITO layer not coated with the CE material but exposed to the electrolyte is electrically separated from the ITO layer in contact with the actual electrodes (Fig. 4a). Secondly, CE–CE cells where an electrical connection between these particular areas of the substrates exists (Fig. 4b). In the latter case the uncoated ITO surface is electrically active in the impedance measurements and has an effect on the impedance spectra of the measurement cell.

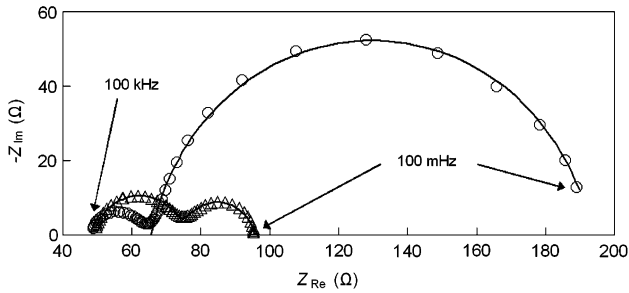


Fig. 2. Typical impedance spectra (Nyquist plots) of the counter electrode cells.  $\Delta$ : carbon powder;  $\circ$ : Sb:SnO<sub>2</sub>+Pt. Solid lines: respective fits. Fitted parameters for carbon powder are (model B in Fig. 4):  $R_{CT} = 10.3 \Omega$ ,  $R_1 = 49.0 \Omega$ ,  $R_2 = 26.3 \Omega$ ,  $B_{EL} = 2.04 \times 10^3 \text{ F}^{-1} \text{ s}^{0.134}$ ,  $\beta_{EL} = 0.866$ ,  $B_{ITO} = 2.22 \times 10^3 \text{ F}^{-1} \text{ s}^{0.143}$  and  $\beta_{ITO} = 0.857$ . Fitted parameters for Sb:SnO<sub>2</sub>+Pt are (model A in Fig. 4):  $R_{CT} = 64 \Omega$ ,  $R_S = 65.8 \Omega$ ,  $CPE_{EL} = 835 \text{ F}^{-1} \text{ s}^{0.126}$ ,  $\beta_{EL} = 0.874$ .

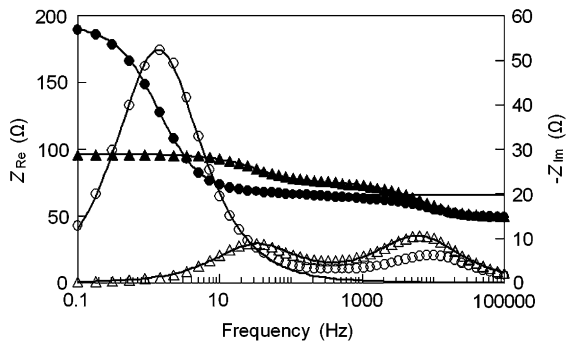


Fig. 3. Impedance spectra, with real and imaginary parts separated, of the same samples as in Fig. 2.  $\blacktriangle$ :  $Z_{Re}$ , carbon powder;  $\bullet$ :  $Z_{Re}$ , Sb:SnO<sub>2</sub>+Pt.  $\Delta$ :  $-Z_{Im}$ , carbon powder;  $\circ$ :  $-Z_{Im}$ , Sb:SnO<sub>2</sub>+Pt. Solid lines: respective fits, with the same parameters as in Fig. 2.

The impedance arc and corresponding peak in the imaginary impedance dominating in the frequency range 100 mHz–500 Hz in the spectra (Figs. 2–3 and Fig. 5) is related to the porous electrodes and is represented by a parallel connected RC circuit consisting of a resistor  $2R_{CT}$  corresponding to the sum of the charge transfer resistances of the electrodes and a constant phase element  $CPE_{EL}$  corresponding to the double layer charging at the porous electrode–electrolyte interfaces of the electrodes. Impedance of the constant phase element is  $Z_{CPE}(\omega) = B(j\omega)^{-\beta}$ , where  $\omega$  is the angular frequency,  $\beta$  is the CPE exponent ( $0 \leq \beta \leq 1$ ) and  $j$  is the imaginary unit. Resistance  $R_S$  (Fig. 4a) accounts for the resistance of the electrically conductive materials in the cell with contributions from the ITO substrate layer, porous electrode material, current collector contacts and resistivity of the electrolyte.

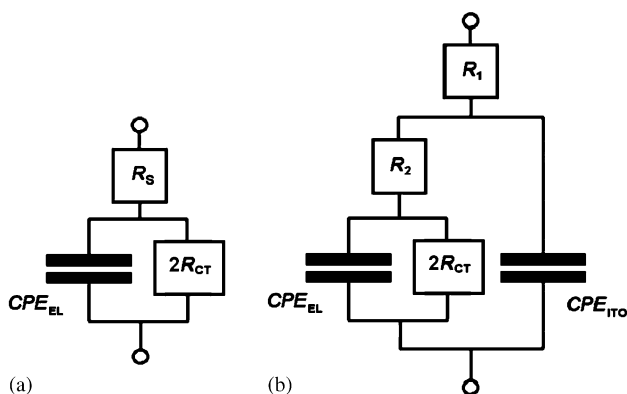


Fig. 4. Equivalent circuit models for the interpretation of the measured impedance spectra from counter electrode cells described in Fig. 1. (a): model excluding the uncoated ITO surface, (b): model including the uncoated ITO surface.

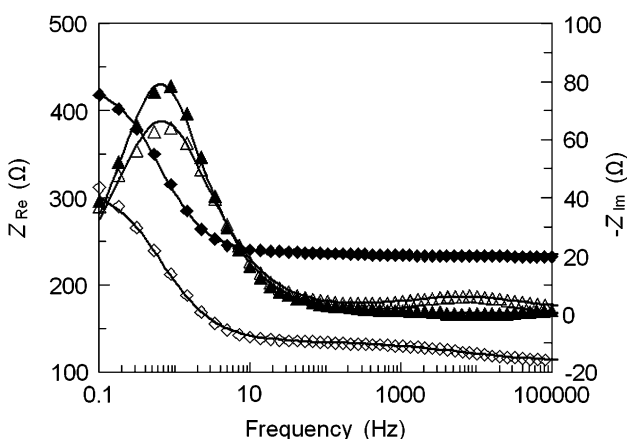


Fig. 5. Measured real and imaginary impedances of cells with and without uncoated ITO.  $\diamond$ :  $Z_{re}$  with ITO,  $\triangle$ :  $-Z_{im}$  with ITO,  $\circ$ :  $Z_{re}$  without ITO,  $\blacktriangle$ :  $-Z_{im}$  without ITO. Solid lines: respective fits. Fitted parameters for the cell with uncoated ITO (model B in Fig. 4):  $R_{CT} = 92 \Omega$ ,  $R_1 = 111 \Omega$ ,  $R_2 = 23.7 \Omega$ ,  $B_{EL} = 612 F^{-1} s^{0.198}$ ,  $\beta_{EL} = 0.802$ ,  $B_{ITO} = 1.09 \times 10^4 F^{-1} s^{0.424}$ ,  $\beta_{ITO} = 0.576$ . Fitted parameters for the cell without uncoated ITO (model A in Fig. 4):  $R_{CT} = 99 \Omega$ ,  $R_S = 235 \Omega$ ,  $B_{EL} = 662 F^{-1} s^{0.142}$ ,  $\beta_{EL} = 0.858$ .

Existence of an impedance arc at higher frequencies 500 Hz–100 kHz corresponds to the situation of Fig. 4b and is related to the capacitance of the uncoated ITO surface that is in contact with the electrolyte in the electrolyte filling channels of the measurement cell and is represented by a constant phase element  $CPE_{ITO}$ . The charge transfer resistance of the uncoated ITO surface is in the megaohm range and can be neglected in the model. In this case the electrical resistance of the cell is divided in two resistors  $R_1$  and  $R_2$  as depicted in Fig. 4b.

The spectra were interpreted assuming both electrodes in a CE–CE cell identical which is justified because the mass and thickness variations between the electrodes of one cell were small enough to not be detected in the impedance spectra.  $R_{CT}$  in Fig. 4 and elsewhere in this paper refers to the charge transfer resistance of a single electrode in the CE–CE cell. All other equivalent circuit components in Fig. 4 refer to the whole measurement cell.

### 3.2. The effect of uncoated ITO–electrolyte interface on the impedance spectra

In the course of the work it was noticed that the presence of uncoated ITO surface in the electrolyte filling channels of the measurement cell induces an additional impedance arc at high frequencies in the impedance spectrum of the cell. This was first hypothesized from the fact that the high frequency arc, in contrast to the low frequency arc, showed no correlation to the electrode properties. The hypothesis was confirmed by using measurement cells where the ITO layer in the electrolyte filling channels was electrically separated from the rest of the substrate by cutting through the ITO layer with a scalpel. Fig. 5 shows a comparison between impedance spectra from cells with and without uncoated ITO surface in electrical contact with the electrode. The electrical separation effectively removed the impedance feature at the high frequencies without affecting the low frequency impedance arc. The small difference in the low frequency arc in Fig. 5 can be explained by difference in electrode thickness and mass.

The fact that the impedance response of the cell was affected by the uncoated ITO–electrolyte interface highlights the importance of an adequately designed measurement cell in EIS studies. We point out that the thin layer cell design used in this work has been common in the experimental studies of DSSCs and their CEs, but the implementation of the electrolyte filling channels has been rarely described in the publications. In case of glass substrates, the electrolyte filling channels have sometimes been prepared by drilling holes through the substrates, e.g. [20]. This is indeed recommended, as it can be used to effectively minimize or eliminate altogether areas of uncoated ITO–electrolyte interface in the cell. Alternatively, the TCO surface layer can be removed by chemical etching or electrically isolated from rest of the electrode, the latter being perhaps more practical in the case of plastic substrates as described above.

Even in the presence of the effect from the uncoated ITO–electrolyte interface the  $R_{CT}$  of the electrode is readily available from the impedance spectra as the real axis diameter of the low frequency arc in the Nyquist plot [2,18,19]. We have therefore also included results where the effect of the uncoated ITO was present. In case the effect was clearly separated from the electrode impedance in the frequency domain, fitting could be performed reliably also to the model of Fig. 4a. The impedance spectrum of the Sb:SnO<sub>2</sub> + Pt and the corresponding fit in Figs. 2–3 serves as an example of this.

We next give qualitatively two likely explanations why the uncoated ITO surface gives rise to an impedance response similar to that of the electrode impedance, i.e. an arc in the Nyquist plot (Fig. 2), and justify the equivalent circuit that takes the effect into account (Fig. 4b).

The effect of the uncoated ITO–electrolyte interface to the impedance spectra can be explained first of all by the geometry of the measurement cell and the distributed resistance in the ITO substrate. The uncoated ITO–electrolyte interface at the electrolyte filling channels functions as an additional current pathway at high frequencies which means that the current distribution in the ITO substrate is frequency dependent. This lowers the measurement cell's apparent series resistance taken as the high frequency limit of  $Z_{Re}$  as also seen in Fig. 5. At high enough frequencies where the electrode–electrolyte interface is shorted by its double layer capacitance, a part of the distributed ITO resistance between the electrode and the electrolyte filling channels acts as a parallel resistance to the capacitance of the uncoated ITO–electrolyte interface. The result is an arc in the Nyquist plot of the impedance spectrum of the cell at high frequencies (Fig. 2).

The effect of the uncoated ITO can be accounted for in the equivalent circuit model. In a detailed equivalent circuit, the distributed resistance of the ITO substrate would be modeled with a resistor network. The same effect can be produced with a simplified equivalent circuit using only two resistors,  $R_1$  and  $R_2$ , as depicted in Fig. 4b. This circuit reproduces the main effects of the uncoated ITO–electrolyte interface: apparent lowering of the series resistance and parallel RC behavior at high frequencies.

The effect of the uncoated ITO–electrolyte interface may also arise from the resistivity of the porous electrode material. This gives the equivalent circuit model in Fig. 4b an alternative interpretation where the resistance  $R_2$  is due to the electrode resistivity. In reality both the electrode resistivity and the distributed resistance in the ITO substrate may contribute to the effect and cannot be quantitatively distinguished from our measurements. However, the sum  $R_1 + R_2$  in the model of Fig. 4b corresponds quantitatively to the series resistance  $R_S$  in the model of Fig. 4a, representing the series resistance of the cell at DC conditions, and  $R_1 + R_2 + R_{CT}$  is the total DC resistance of the cell at small polarizations.

### 3.3. Discussion of the electrode impedance

Features in the impedance spectra of electrochemical systems are related to physicochemical processes, such as charge transfer and transport or chemical reactions, occurring in the system when electric current passes through it [21,22]. Processes identified in the impedance spectra of CEs of DSSCs include double layer charging and charge transfer at the electrode–electrolyte interface, diffusion of ions in the electrolyte, and pure electric conduction in the materials [2,18].

In case of Pt CEs prepared on FTO glass, two impedance arcs are seen in the impedance spectra with organic liquid electrolytes: the charge transfer impedance at the electrode–electrolyte interface in the frequency range 100 Hz–100 kHz, and finite length Warburg diffusion impedance [21] in the frequency range 1–10 Hz [18,19]. In contrast to this, the compressed powder electrodes exhibited only one true impedance arc that appeared in the frequency range 0.1–10 Hz for the Sb:SnO<sub>2</sub> + Pt

electrodes and 5–500 Hz for the compressed carbon powder electrodes. We identified this as the charge transfer impedance of the electrode (Fig. 2). Its appearance at relatively low frequencies and insignificant contributions from diffusion impedance can be explained by the porous nature of these electrodes.

The characteristic frequency  $f^*$  of a parallel RC circuit is given by  $f^* = (2\pi RC)^{-1}$ , where  $R$  is resistance and  $C$  the capacitance [22]. Due to higher active surface area, the capacitance of the compressed porous CEs studied here is ca. two orders of magnitude larger than that of planar Pt electrodes. This explains why the charge transfer impedance of the compressed powder electrodes appears at much lower frequencies than that of a planar Pt electrode with the same charge transfer resistance and with the same or similar electrolyte used in the measurements.

A property of the finite length Warburg diffusion impedance is that as the thickness of the electrolyte layer decreases the diffusion impedance is confined to higher frequencies and decreases in magnitude [21]. The thickness of the free electrolyte layer between the electrodes was typically a few tens of micrometers in our measurement cells. To facilitate quantitative discussion, the expected diffusion impedance for a planar electrode cell was calculated using the electrolyte concentrations given in Section 2.5 and a diffusion coefficient  $D = 3.6 \times 10^{-6} \text{ cm}^2/\text{s}$  for all ions in the electrolyte [18] taking into account both triiodide and iodine diffusion [21]. For 10, 20 and 50  $\mu\text{m}$  thick free electrolyte layers, the magnitude of the imaginary component of the diffusion impedance had a maximum value of 1.1  $\Omega$  (at 6 Hz), 3.1  $\Omega$  (at 0.65 Hz) and 5.1  $\Omega$  (at 0.25 Hz), respectively. The frequency range of the planar electrode diffusion impedance at these typical electrode separations would thus overlap with the charge transfer impedance of the Sb:SnO<sub>2</sub>+Pt electrodes, but would be much smaller in magnitude compared to it (Fig. 3).

In addition, porous electrodes exhibit generally lower mass transfer overpotentials than their planar equivalents because the porosity tends to even out any large variations in the ion concentrations in the pores of the electrode as a result of balance between mass transfer and kinetic overpotentials [5]. The contribution of diffusion in the electrolyte to the impedance spectra of the compressed powder electrodes studied here can therefore be considered negligible. No signs of diffusion impedance were observed in the spectra from compressed carbon powder electrodes at the frequency range calculated above, which provides experimental support for this conclusion (Fig. 3).

We finally note that because of the porous nature of the electrodes, the charge transfer resistance determined in this study is not purely a measure of the electrocatalytic activity (i.e. exchange current density) at the electrode–electrolyte interface on the microscopic level, but includes also contributions from the resistivities of the porous electrode material and the electrolyte in the pores [23]. The charge transfer resistance determined using the equivalent circuit models of Fig. 4 should therefore be taken as an overall or effective polarization resistance of the electrode. Effect of the electrode resistivity on the performance of the porous CEs is a subject of our ongoing research.

### 3.4. Charge transfer resistances and comparison to literature

The optimum choice for the CE-type and materials is a matter of performance, cost and durability of the electrode. In this study the performance of the CEs was investigated in terms of the overall charge transfer resistance between the electrode and the electrolyte. The best obtained charge transfer resistances and corresponding electrode thicknesses for the electrode materials studied in this research, along with their comparison to the results obtained by other groups, are presented in Table 1.

The iodine/triiodide reduction kinetics at the CE depend on the ion concentrations and solvent used in the electrolyte, the charge transfer resistance being generally larger the higher the viscosity of the solvent and the lower the ion concentrations [2,18,22]. Direct comparison of the  $R_{CT}$  results obtained here is therefore not possible to studies where markedly different electrolyte composition was used [2,5,14,24] or the composition was not given [25]. However, compared to our own reference samples prepared by thermal platinization method on FTO glass substrates, and, compared to the results obtained by others, the performance of the compressed carbon powder CEs on flexible ITO–PET was very good, and that of the platinized Sb:SnO<sub>2</sub> ones satisfactory as well.

The charge transfer resistance is the slope of the kinetic current density–overpotential relation at zero polarization of the electrode–electrolyte interface. Because the current density increases exponentially as a function of the kinetic overpotential as described by the Butler–Volmer equation [22], the  $R_{CT}$  gives an upper limit to the kinetic voltage losses at the CE at non-zero polarizations. If the electrodes were used in a typical DSSC, for example, a cell with 5% efficiency and operating parameters  $i_{SC} = 17 \text{ mA/cm}^2$ ,  $V_{MPP} = 0.4 \text{ V}$  and  $i_{MPP} = 12.6 \text{ mA/cm}^2$  at  $100 \text{ mW/cm}^2$  AM1.5G

Table 1  
Comparison between the charge transfer resistances obtained in this study and the results obtained in other studies

CE type	Electrode thickness	$R_{CT}$ ( $\Omega \text{ cm}^2$ )	Ref.
Sputtered Pt	2–3 nm	57	[18] <sup>a</sup>
Sputtered Pt	> 2 nm	0.8–2.1	[19] <sup>b</sup>
Sputtered Pt	4–70 nm	1–11	[10] <sup>c</sup>
PEDOT-TsO	1.5 $\mu\text{m}$	0.4–0.5	[10] <sup>c</sup>
Thermal Pt	N/A	4–5	This study <sup>d</sup>
Sb:SnO <sub>2</sub> + Pt	20–40 $\mu\text{m}$	8–13	This study <sup>d</sup>
	1.1–2.3 nm (Pt) <sup>e</sup>		
Carbon powder	10–20 $\mu\text{m}$	0.5–2	This study <sup>d</sup>

TBP = 4-*tert*-butyl pyridine.

DMPH = 1,2-dimethyl-3-propylimidazolium iodine.

Electrolyte compositions used:

<sup>a</sup>0.5 M LiI + 0.05 M I<sub>2</sub> + 10 vol% TBP in 3-methoxypropionitrile.

<sup>b</sup>0.1 M LiI + 0.6 M DMPH + 0.1 M I<sub>2</sub> + 0.5 M TBP in 3-methoxypropionitrile.

<sup>c</sup>0.1 M LiI + 0.3 M DMPH + 0.05 M I<sub>2</sub> + 0.5 M TBP in methoxyacetonitrile.

<sup>d</sup>0.5 M LiI + 0.05 M I<sub>2</sub> + 0.5 M (7.4 vol%) TBP in 3-methoxypropionitrile.

<sup>e</sup>Corresponding thickness of a planar crystalline Pt layer with the same Pt surface density.

equivalent light intensity (a cell prepared on glass substrates in our laboratory), the charge transfer resistances measured with the carbon powder would cause a voltage loss of only 8.5–34 mV under short-circuit conditions, and an efficiency loss of only 1.6–6.3% if the cell was used at the maximum power point. For the Sb:SnO<sub>2</sub>+Pt CEs the corresponding values would be 136–221 mV under short-circuit, and 25.2–41.0% at the maximum power point. These results show that room for development still exists for platinized Sb:SnO<sub>2</sub>, while the charge transfer resistance of the carbon powder looks very promising already as it is.

The very low  $R_{CT}$  obtained with the carbon powder electrodes suggests that this type of CE could be even suitable for high efficiency dye solar cells operating at current densities up to 20 mA/cm<sup>2</sup> at full sunlight, inasmuch as the mass transport overpotential at these porous electrodes is expected to be lower and the limiting current density in the thin layer cell configuration higher than those of a planar CE with the same effective  $R_{CT}$ . However, a larger separation between the cell substrates may be needed in practice with thick porous electrodes than with planar Pt electrodes. As shown by Papageorgiou et al. [5], increasing the electrode separation can increase the overpotential at the photoelectrode and reduce the injection rate of photoelectrons due to local decrease in iodide concentration. This point should be considered in addition to a low  $R_{CT}$  when targeting high current densities with the porous CEs.

The amount of expensive platinum should be minimized in an economically optimized CE, but without sacrificing its kinetic performance. The required platinum loading of the electrode in the thermal platinization method is optimally as low as 5 μg/cm<sup>2</sup> [2], which in terms of Pt consumption is equivalent to a 2.3 nm thick planar crystalline Pt layer. Also with sputtering a few nanometers of platinum is usually enough [20,21]. In this study the 20–40 μm thick Sb:SnO<sub>2</sub>+Pt electrodes had approximately 2.5–5.0 mg/cm<sup>2</sup> surface density of the electrode powder material containing approximately 0.098% Pt by weight. This means that the studied Sb:SnO<sub>2</sub>+Pt electrodes had Pt loading equivalent to 1.1–2.3 nm of planar crystalline Pt layer. With regard to the achieved  $R_{CT}$  results (Table 1) the Sb:SnO<sub>2</sub>+Pt electrodes in this study showed therefore effective utilization of the electrocatalytic activity of the Pt included in the electrode, when compared to the results obtained by others with sputtered Pt layers [10,18,19].

### 3.5. Other observations

After initial screening, three large series (up to 200 samples) of electrodes were made to understand the correlation between the manufacturing process and electrode characteristics, i.e. thickness, mass and evenness, and the repeatability of the process. The thickness and mass were easy to control by simply altering the spraying time. Compacting by compressing led to even and mechanically stable film quality, especially for the platinized Sb:SnO<sub>2</sub> electrodes, inasmuch as the films adhered well to the substrate without flaking off. The Sb:SnO<sub>2</sub>+Pt films were more durable than the carbon powder films at high film thicknesses. When the thickness of the carbon powder electrodes exceeded about 40 μm, the electrode material tended to flake off from the substrates, but thinner electrodes showed proper durability to be used in the cells.

Preliminary measurements showed that the grinding time of the mixture was a crucial manufacturing parameter for the carbon powder electrodes. Less than 15 min grinding time led to electrodes with poor adherence on the substrates and large charge transfer resistances ranging from ca.  $70 \Omega \text{cm}^2$  to as high as several hundred  $\Omega \text{cm}^2$ . Non-platinized Sb:SnO<sub>2</sub> electrodes' charge transfer resistances were also several hundred  $\text{k}\Omega \text{cm}^2$ .

During the work, large scattering was observed in the correlation between measured electrode masses and  $R_{\text{CT}}$ . By weighing a set of reference samples at different relative humidity (RH) conditions at room temperature it was noticed that the substrate material adsorbed considerable amounts of water from the air. The correlation between RH and the measured mass was  $1 \mu\text{g}/\text{cm}^2$  of ITO–PET substrate area per 1% RH.

#### 4. Conclusions

The results obtained here show that low temperature spray deposition followed by compacting by compression is a promising manufacturing technique for DSSC CEs made of alternative materials, i.e. materials other than platinum on glass substrate.

Porous, conductive carbon powder or platinized Sb-doped SnO<sub>2</sub> CEs sprayed and compressed on conductive plastic substrates showed satisfactory mechanical stability. Their charge transfer resistances were close to those of thermal platinum on FTO glass. Carbon powder electrodes gave the best results,  $0.5\text{--}2 \Omega \text{cm}^2$ , compared to the reference values of  $4\text{--}5 \Omega \text{cm}^2$  obtained with thermal Pt on FTO glass. Manufacturing of a large series of even quality electrodes was demonstrated. In addition, the physical parameters, i.e. thickness, mass and shape of the electrodes, were simple to control with the spraying method. This makes the approach used interesting for industrial-scale manufacturing.

#### Acknowledgements

Financial support from the National Technology Agency of Finland (Tekes) is gratefully acknowledged. J. H. is grateful for the scholarship from the Nordic Energy Research (NEFP). The authors thank Dr. Jani Kallioinen for supplying the ITO–PET substrates for the study, Degussa for the carbon black and TiO<sub>2</sub> samples, Milliken Chemicals for the Sb:SnO<sub>2</sub> sample, Dupont for the Surlyn sheets and Mr. Christian Orassaari and Mr. Harri Jaronen for performing compaction of the powder electrodes.

#### References

- [1] M.K. Nazeeruddin, A. Kay, I. Rodicio, R. Humphry-Baker, E. Müller, P. Liska, N. Vlachopoulos, M. Grätzel, *J. Am. Chem. Soc.* 115 (1993) 6382–6390.
- [2] N. Papageorgiou, W.F. Maier, M. Grätzel, *J. Electrochem. Soc.* 144 (1997) 876–884.

- [3] A. Kay, M. Grätzel, *Solar Energy Mater. Solar Cells* 44 (1996) 99–117.
- [4] S. Burnside, S. Winkel, K. Brooks, V. Shklover, M. Grätzel, A. Hinsch, R. Kinderman, C. Bradbury, A. Hagfeldt, H. Pettersson, *J. Mater. Sci. : Mater. Electron.* 11 (2000) 355–362.
- [5] N. Papageorgiou, P. Liska, A. Kay, M. Grätzel, *J. Electrochem. Soc.* 146 (1999) 898–907.
- [6] K. Imoto, K. Takahashi, T. Yamaguchi, T. Komura, J. Nakamura, K. Murata, *Solar Energy Mater. Solar Cells* 79 (2003) 459–469.
- [7] K. Suzuki, M. Yamaguchi, M. Kumagai, S. Yanagida, *Chem. Lett.* 32 (2003) 28–29.
- [8] T. Kitamura, M. Maitani, M. Matsuda, Y. Wada, S. Yanagida, *Chem. Lett.* (2001) 1054–1055.
- [9] Y. Saito, T. Kitamura, Y. Wada, S. Yanagida, *Chem. Lett.* (2002) 1060–1061.
- [10] Y. Saito, W. Kubo, T. Kitamura, Y. Wada, S. Yanagida, *J. Photochem. Photobiol. A: Chem.* 164 (2004) 153–157.
- [11] Y. Shibata, T. Kato, T. Kado, R. Shiratuchi, W. Takashima, K. Kaneto, S. Hayase, *Chem. Commun.* (2003) 2730–2731.
- [12] K.C. Mandal, A. Smirnov, D. Peramunage, R.D. Rauh, *Mater. Res. Soc. Symp. Proc.* 737 (2003) 739–744.
- [13] S.A. Haque, E. Palomares, H.M. Upadhyaya, L. Otley, R.J. Potter, A.B. Holmes, J.R. Durrant, *Chem. Commun.* 24 (2003) 3008–3009.
- [14] C. Longo, J. Freitas, M. De Paoli, *J. Photochem. Photobiol. A: Chem.* 159 (2003) 33–39.
- [15] T. Ma, X. Fang, M. Akiyama, K. Inoue, H. Noma, E. Abe, *J. Electroanal. Chem.* 574 (2004) 77–83.
- [16] X. Fang, T. Ma, M. Akiyama, G. Guan, S. Tsunematsu, E. Abe, *Thin Solid Films* 472 (2005) 242–245.
- [17] H. Lindström, A. Holmberg, E. Magnusson, S. Lindquist, L. Malmqvist, A. Hagfeldt, *Nano Lett.* 1 (2001) 97–100.
- [18] A. Hauch, A. Georg, *Electrochim. Acta* 46 (2001) 3457–3466.
- [19] X. Fang, T. Ma, G. Guan, M. Akiyama, T. Kida, E. Abe, *J. Electroanal. Chem.* 570 (2004) 257–263.
- [20] L. Dloczik, O. Ieperuma, I. Laueremann, L.M. Peter, E.A. Ponomarev, G. Redmond, N.J. Shaw, I. Uhlendorf, *J. Phys. Chem. B* 101 (1997) 10281–10289.
- [21] J.R. Macdonald, *Impedance Spectroscopy : Emphasizing Solid Materials and Systems*, Wiley, New York, 1987.
- [22] A.J. Bard, L.R. Faulkner, *Electrochemical Methods: Fundamentals and Applications*, Wiley, New York, 2000.
- [23] J.S. Newman, *Electrochemical Systems*, Prentice Hall, Englewood Cliffs, NJ, 1991.
- [24] C. Longo, A.F. Nogueira, M.-A. De Paoli, H. Cachet, *J. Phys. Chem. B* 106 (2002) 5925–5930.
- [25] N. Papageorgiou, *Coord. Chem. Rev.* 248 (2004) 1421–1446.